Protonation-state dependent Communication in Cytochrome c Oxidase

Mahdi Bagherpoor Helabad,[†,§] Tahereh Ghane[§],[†,§] Marco Reidelbach,[†] Anna Lena Woelke,[‡] Ernst Walter Knapp,[¶] and Petra Imhof[*,†]

†*Institute of Theoretical Physics, Free University Berlin, Arnimallee 14, D-14195 Berlin*

‡*Institute of Pharmacy, Free University Berlin, Königin-Luise-Strasse 2+4, D-14195 Berlin*

¶*Institute of Biochemistry, Free University Berlin, Takustr. 6, D-14195 Berlin*

§*These authors contributed equally.*

E-mail: petra.imhof@fu-berlin.de

Abstract

Proton transfer in Cytochrome c oxidase (CcO) from the cellular inside to the binuclear redox center (BNC) can occur through two distinct pathways, the D- and K-channel. In order for the protein to function as both, redox enzyme as well as proton pump, proton transfer into the protein towards the BNC or towards a proton loading site, and ultimately through the membrane, must be highly regulated. The $P_R \rightarrow F$ transition is the first step in its catalytic cycle that requires proton transfer from the bulk at the N-side to the BNC. Molecular dynamics simulations of the $P_R \rightarrow F$ intermediate of this transition, with sixteen different combinations of protonation states of key residues in the D- and K-channel show the impact of the K-channel on the D-channel to be protonation state dependent. Both, strength as well as means of communication, correlations in positions or along the hydrogen-bonded network, depend on the protonation state of the K-channel residue K362. The conformational and hydrogen bond dynamics of the D-channel residue N139 is regulated by an interplay of protonation in the D-channel and K362. N139 thus assumes a gating function by which proton passage through the D-channel towards E286 is likely facilitated for states with protonated K362 and unprotonated E286. In contrast, proton passage through the D-channel is hindered by N139's preference for a closed conformation in situations with protonated E286.

Introduction

Cytochrome c Oxidase (CcO), is a member of the large family of heme-copper oxidases. It is also known as Complex IV, because of its role as an enzyme of the respiratory chain, reducing molecular oxygen to water by taking up electrons and protons from the P- and N-side of the membrane, respectively[1]. Four protons are consumed in the reduction reaction of dioxygen to water. Four additional protons are pumped across the mitochondrial or bacterial membrane. In CcO of type A, all protons are supposed to enter through two channels, the D- and K-channel, named after D132 at the entrance of the first, and K362 as the key residue of the latter channel, respectively (*Rhodobacter sphaeroides* numbering). The D-channel connects the N-side of the membrane to E286, located ∼10 Å from the binuclear center (BNC), i.e. the site of oxygen reduction. The K-channel spans from E101 on the N-side to Y288 at the binuclear center. Both channels consist of a combination of polar residues and, given the necessary amount of water inside the channels, hydrogen bonded networks enabling proton transfer into the protein's interior.

The D-channel has been suggested to be the predominant pathway for provision of protons via E286 required in the reductive phase of the oxidase reaction to compensate for the electrons being transferred to heme a. The K channel is thus discussed to allow heme *a3* reduction and oxygen binding by enabling proton transfer to Y288 at the BNC. Mutation studies and biochemical experiments have shown that the Lysine of the K-channel likely plays an active role by conducting protons rather than only providing positive charge in the vicinity of Y288. However, the substrate protons transported through the K-channel are required only in the reductive phase of the catalytic cycle. The remaining substrate protons required in the oxidative phase (P→-F→O) are thought to be supplied via the D-channel[2–4]. According to other suggestions, all protons consumed in the oxygen-to-water conversion chemistry are delivered through the K-channel[5] and a mechanism for gating the K-channel has been proposed in Ref. 6. In contrast, there is a consensus that all pumped protons are transferred through the D-channel.

Crystal structures show K362 pointing "down" towards the N-side not connecting to the BNC,

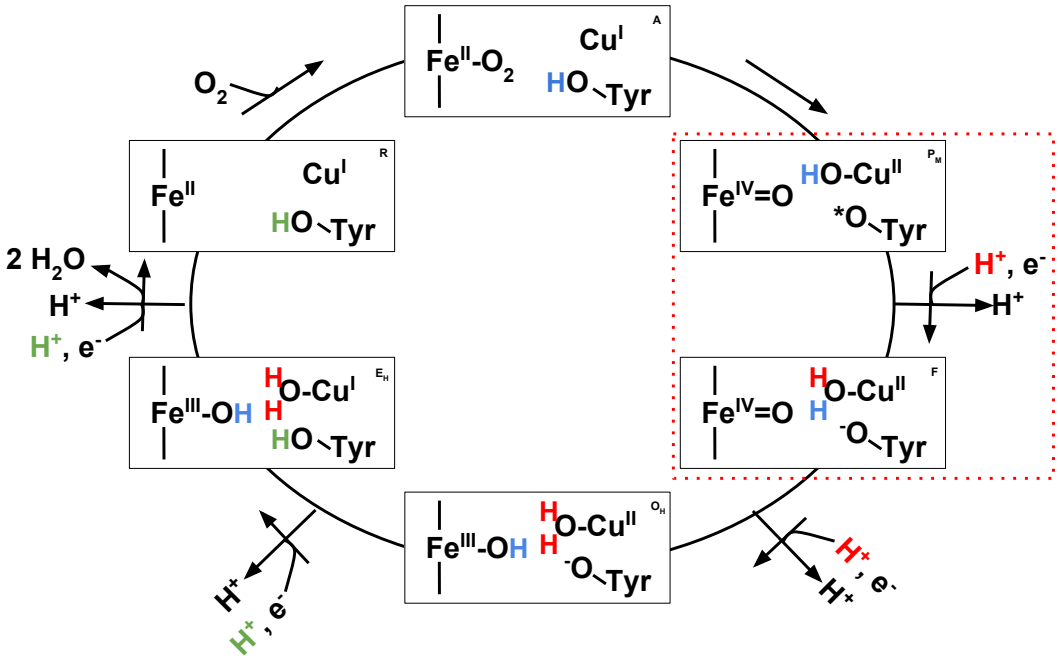

Figure 1: Catalytic cycle of cytochrome c oxidase. The fully reduced state R binds an oxygen atom resulting in state A. The O-O bond is cleaved in state P. Via four subsequent steps (P→F→O→E→R) electrons are taken from the P-side and protons from the N-side of the membrane, ultimately reducing one oxygen molecule to two water molecules per cycle.

and insufficient water molecules are resolved to bridge this gap[7–9]. However, molecular dynamics simulations have shown that protonated K362 can move towards the BNC whereas neutral K362 is unlikely to do so[10,11]. According to pKa calculations of CcO in different redox states[11], in the reductive half of the catalytic cycle K362 is likely transiently protonated in the intermediate states O→E and E→R whereas the P_R →F intermediate is the only one in the oxdative half in which protonation of K362 is likely[11]. Regarding the reductive half, the conformational rearrangement of K362 has been argued to close the K-pathway for (further) proton transfer during oxygen reduction[12], ensuring that no protons are transferred directly to the catalytic site and thus preventing uptake of protons which are supposed to be pumped. However, simulations of CcO with protonated K362 indicate an increased amount of water molecules inside the K-channel that may enable proton transfer through the K-channel[11]. In the oxidative phase, the "up"-orientation of K362 may only serve to compensate additional negative charge at the BNC, thereby facilitating the formation of the P_R →F intermediate with a tyrosinate (Y288) but not further transfer of a proton from K362 to Y288 due to the low proton affinity of Y288[13]. The additional eletron at the BNC has lead to the P_R state being considered as a "high energy" state[14] and, consequently, the proton transfer coupled to the P_R→F transition proceeds energetically "downhill".

Here, we investigate the situation in which the first electron has arrived at the BNC and the first proton transitions from the bulk to the protein interior take place, represented by the P_R →F intermediate state with a negatively charged Y288. For the proton tranfer through the D-channel, the protonation states of D132 at the channel entrance and E286 at the channel exit are obviously important. However, the protonation state of K-channel residues K362 and E101 of subunit II, which has been discussed as a possible entry point of the K-channel[15,16], may also have an impact on proton transport through the D-channel.

In this work we use molecular dynamics simulations to analyze the communication within and between protein residues of the D- and K-channel in order to elucidate whether and how a change of protonation state of the key residues is "sensed" by the other key residues and possibly results

in an altered conformational and hydrogen-bond dynamics that ultimately changes the proton transfer probability.

Methods

Molecular dynamics simulations

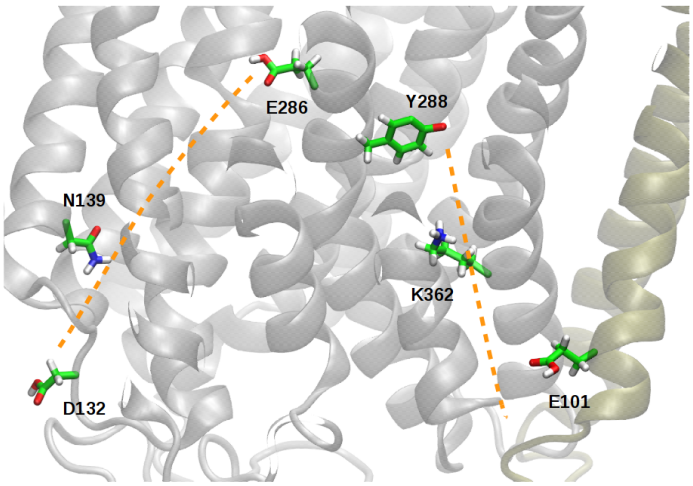

D132	E286	K362	E101
0	0	0	0
0	0	0	1
0	1	0	0
0	1	0	1
1	0	0	0
1	0	0	1
1	1	0	0
1	1	0	1
0	0	1	0
0	0	1	1
0	1	1	0
0	1	1	1
1	0	1	0
1	0	1	1
1	1	1	0
1	1	1	1

Figure 2: Left: Lower part of cytochrome c oxidase highlighting important residues of the D- and K-channel, respectively. The proton transfer channels are indicated by dashed lines. For residues D132, E286, K362, and E101 the protonation states have been varied in the present study. The figure shows the 1111 model with all four residues protonated. Right: Simulated protonation states of cytochrome c oxidase. "1" refers to a proton at the respective residue, leading to a protonated lysine, or neutral aspartate and glutamate residues, respectively. "0" indicates no such proton, corresponding to neutral lysine or negatively charged aspartate or glutamate, respectively.

The model setup follows the same protocol as described in Ref. 11. For protein residues the CHARMM22 force field[17] was applied, while the parameters for the cofactors are based on quantum chemically derived atomic partial charges and optimized cofactor geometry by Woelke et al.[11]. The core enzyme complex was embedded in a lipid bilayer of phosphatidylcholines and solvated in TIP3 water[18] (∼115000 atoms in total). Parameters for the lipid bilayer were obtained from the CHARMM36 extension for lipids[19]. Heme a3 was modelled with Fe(IV) bound to one oxygen atom ("half an oxygen molecule") and the copper(II)B-ion was modelled bound to a hydroxyl ion. Y288 was modeled in the deprotonated state. This setup as well as charges and bonds to ligands is the same as described in Ref. 11. Na^+ counter-ions were added by random substitution of water oxygen atoms to neutralize the charge of the system.

The protonation states for the key residues of the two channels, D132, E286, K362, and E101 were varied in all possible combinations resulting in a total of 16 models (see Fig 2). We refer to the differently protonated models by a binary number indicating the protonation state of the four key residues as "1" if protonated and as "0" if not. Model 1010, for example has D132 and K362 protonated, but E286 and E101 unprotonated.

Simulations were performed using periodic boundary conditions in a tetragonal box of size (x=y=96 Å, z=124 Å). Long-range electrostatic interactions were treated using the Particle Mesh Ewald method[20] on a 96 x 96 x 128 charge grid. A non-bonded cutoff of 12 Å was applied. The short range electrostatics and van der Waals interactions were truncated at 12 Å using a switch function starting at 10Å.

The solvated structures were minimized using 5000 steps of steepest descent, then gradually heated for 30 ps to 300 K with 1 K temperature steps with harmonic restraints on the solute atoms.

The systems were equilibrated in three different stages with the numbers of particles, pressure (1 bar) and temperature (300 K) kept constant (NPT ensemble) during 75 ps. Pressure control was introduced using the Nosé-Hoover Langevin piston with a decay period of 500 fs. After

equilibration, for all sixteen models, the restraints were lifed and four individual NPT production runs, started with different initial velocities, were performed for 100 ns each. This way, a total simulation time for all models and all MD runs of 6.4 μs was obtained. The integration time step was 2 fs and coordinates were saved with a sampling interval of 2 ps. All covalent bond lengths involving hydrogen atoms were fixed using SHAKE algorithm[21]. For all analyses only the last 60ns of each simulation run were considered.

The Molecular Dynamics (MD) simulations have been carried out using the program NAMD2.9[22]. Simulations have been performed on the ZEDAT cluster (soroban) of the Free University Berlin, and using resources of the North-German Supercomputing Alliance (HLRN). All analyses have been performed on the local linux computers of the physics department.

Conformational Analysis

Distributions of side chain dihedral angles of residues D132, N139, E286, K362, and E101, and distances between those residues have been extracted from the MD simulations of the different protonation models (See supplementary figure S12 for the definition of the side chain dihedral angles). For the distances atoms $C\gamma$, $C\gamma$, $C\delta$, $N\zeta$, and $C\delta$ have been considered for D132, N139, E286, K362, and E101, respectively. From the time series of the distances and dihedral angles, histograms were extracted so as to analyze which dihedral conformational states are occupied in which protonation model and which are the most probable distances. Errors are estimated by averaging over the four individual runs for each protonation model and computing the standard deviation from the mean.

Generalized Correlation

For the generalized correlation analysis, only the protein and 100 water molecules that are inside or close to the D and K channel have been taken into account. For protein residues the center of mass movement has been considered while for the water molecules the movement of the oxygen

atom was used.

Structure snapshots were extracted at $8ps$ interval for all sixteen different protonation state models of CcO. The rotational and translational motions were removed by aligning each snapshot to the median structure of the respective simulation. Furthermore, to reduce the noise level, correlation of residues whose centers of mass (or oxygen atoms for water molecules) are more than 12.0 Å apart in more than 50% of the simulation time is set to zero.

The generalized correlation of centers of mass positions has been computed based on mutual information following an approach put forward by Lange and Grubmüller[23]:

The generalized correlation coefficient, $r_{MI}[x_i, x_j]$, using the entropy space of a bivariate normal distribution for two random variables, x_i and x_j, is defined as

$$r_{MI}[x_i, x_j] = (1 - e^{-2I_{ij}/d})^{1/2} \tag{1}$$

where d is the dimensionality of the vector space, and I_{ij} is the mutual information[24]

$$I_{ij} = H(x_i) + H(x_j) - H(x_i, x_j) \tag{2}$$

Here, x_i and x_j are the positions of centers of mass of residues. The mutual information is estimated from the average distance to the k-nearest-neighbors(kNN), averaged over all x_i or x_j for marginal entropies $H(x_i)$ and $H(x_j)$, or both for joint entropy $H(x_i, x_j)$. The kth neighbor distance algorithm was implemented using nearest neighbor parameter $k = 6$ as described by Kraskov and co-workers[25].

Communication Analysis

The communication analysis has been performed using two metrics for communication, the generalized correlation between residues (see section generalized correlation), or hydrogen-bond connections. For each metric a communication matrix is set up.

In case of the generalized correlation the generalized correlations coefficients $r_{MI}[x_i, x_j]$ are directly used as the matrix elements.

The matrix with hydrogen bond connections is constructed in the following way: For each frame in the MD simulation pairs of residues are checked for hydrogen-bonded connections. An unweighted, undirected hydrogen bonds graph is set up where the residues form the vertices and an edge represents the existence of a hydrogen bond between two residues, based on geometric criteria. On this graph, for each pair of protein residues, the shortest path is determined. If no such path exists, this connection has a count of zero. Direct hydrogen bonds between residues are counted with one. All other hydrogen bonded connections, via auxiliary residues (other protein residues or water molecules) are counted by the inverse of the path length, i.e. the number of hydrogen bonds along the connection. The simulation average of such a count then serves as the respective matrix entry.

For the communication analyses, the matrices were converted into a weighted graph. The protein and water residues are the graph vertices (nodes) and an edge is set between any pair of non-consecutive residues i, j whose corresponding matrix element M_{ij} is non zero. The edge weights, $w(v_i v_j)$, are defined as $w(v_i v_j) = -\ln(M_{ij})$, representing the cost of communication between node v_i and node v_j.

Communication pathways were identified by computing shortest paths on the graph between pairs of nodes (v_1, v_n) using Dijkstra's algorithm[26] where the path length is the sum of the edge weights $\sum_{k=1}^{n} -\ln(M_{k,k+1})$ along that path $P(v_1, \ldots, v_n)$.

The communication analysis has been performed using our own Java-written code, which is based on the JGraph library[27].

Errors for shortest paths along hydrogen-bond connections and correlations, respectively, are estimated by averaging over the respective shortest path lengths computed from the four individual runs for each protonation model and calculated the standard deviation from the mean.

Hydrogen Bond Dynamics

The molecular dynamics simulations were analyzed to quantitatively characterize the dynamics of hydrogen bonds in terms of hydrogen bond time-autocorrelation functions and hydrogen bond life times. The methodology is proposed by Stillinger[28] and developed later by Luzar and Chandler[29].

A hydrogen bond between an acceptor and donor pair is defined in terms of conventional geometric criteria: The distance between the acceptor and donor forming a hydrogen bond must be less than 3.5 Å while the angle between acceptor donor and hydrogen atom should be less than 35° [30,31].

The mean lifetimes of hydrogen bonds between selected protein residues and water molecules are estimated by calculating the time-dependent autocorrelation function, reflecting the presence/absence of hydrogen bonds between all possible donor-acceptor residue pairs [32]. We analyze so-called continuous hydrogen bond life times, in which a specific hydrogen bond is allowed to break and re-form. Defining a binary function $h\,(t)$, which is 1 when a hydrogen bond is present and 0 otherwise[29], the autocorrelation function $C(t)$ of $h\,(t)$ is computed and averaged over similar types of hydrogen bonds, in this work hydrogen bonds between key protein residues (D132, N139, E286, Y288, K362, and E101) and water molecules.

The kinetics of hydrogen bond breakage and re-formation is then derived from this autocorrelation function [29]. Here, a forward rate constant k_{break} for hydrogen bond breakage and a backward rate constant k_{form} for hydrogen bond formation are determined from the reactive flux correlation function

$$K(t) = -\frac{dC(t)}{dt} \tag{3}$$

according to

$$K(t) = k_{break} \cdot C(t) - k_{form} \cdot n(t) \tag{4}$$

where $n\,(t)$ is the probability that a hydrogen bond that existed at $t = 0$ is broken but the donor and acceptor atoms are still within hydrogen bonding distance at time t.

The hydrogen bond lifetime τ^{HB} in this scheme is then given by[33]

$$\tau^{HB} = \frac{1}{k} \tag{5}$$

In this work the dynamics of hydrogen bonds between water molecules and protein residues are evaluated in terms of the autocorrelation function and life times. We have dissected the types of hydrogen bonds into those in which a protein residue is engaged in one, two, three, four, or five hydrogen bonds with water molecules. For each such hydrogen bond state, the binary function $h\,(t)$ is constructed as a time series of ones and zeros for the presence or absence of that state, respectively. For each of the five hydrogen-bond states, then an autocorrelation function has been computed (up to a lag time of 2000ps) from which life times for hydrogen-bond states with one, two, ... five hydrogen bonds were obtained. We have then calculated an effective hydrogen bond life time by taking the average over the life times of the different hydrogen-bond states, weighted by the number of hydrogen bonds of that state. This ansatz takes into account that any hydrogen bond may have an impact on the protonation dynamics, and hence function in CcO, and the simultaneous formation of five hydrogen bonds in principle offers a five times higher chance for proton transfer than a single hydrogen bond.

For each correlation time t we have averaged over the corresponding values of the hydrogen-bond autocorrelation functions C(t) calculated from the four individual simulations. Hydrogen bond life times τ_{break} of the different hydrogen-bond states have then been obtained by fitting a

double exponential function according to

$$C(t) \approx A_1 exp(t/\tau_{break}) + A_2 exp(t/\tau_{form})) \tag{6}$$

from which the mean effective hydrogen bond life times were computed.

Error estimates are obtained as the standard deviation, computed for the individual simulation runs, from the mean values of the effective hydrogen bond life times.

Results

Hydrogen bond dynamics

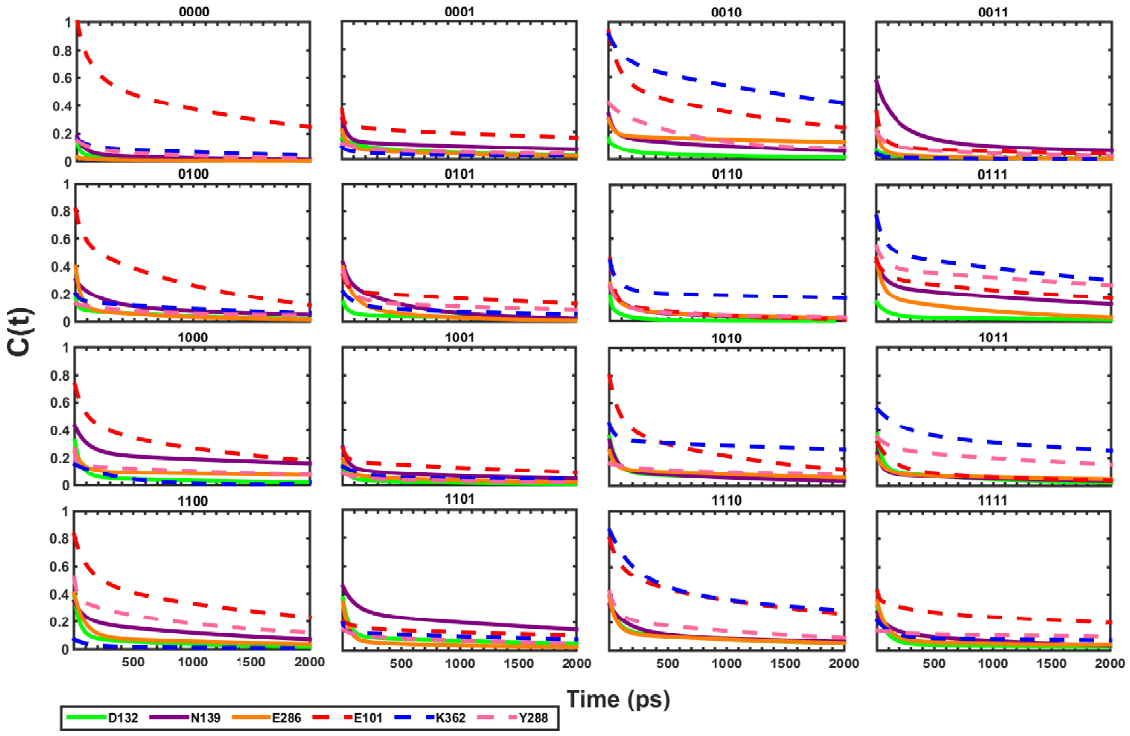

Figure 3: Autocorrelation function, $C(t)$, fitted to life times of effective hydrogen bonds between water molecules and main residues in D-channel (solid lines) and K-channel (dashed lines with symbols) of Cytochrome C Oxidase as a function of time: D132 green, N139 purple, E286 orange, Y288 pink, K362 blue, and E101 red. The protonation models are labeled by "1" for protonated and "0" for unprotonated D132, E286, K362, and E101, respectively.

Figure 3 shows the hydrogen bond dynamics between key residues and water molecules as their decay of the autocorrelation function $C(t)$ fitted to the effective hydrogen bond life times (see Table S1). The hydrogen bond life times for D132 in the different models are rather diverse (with large deviations between individual runs in some cases) and show no clear effect on the protonation state of D132 itself. In models with protonated K362, the hydrogen bond life times with D132 are either similar or reduced compared to models with unprotonated K362. In the presence of protonated E286, additional protonation of D132 decreases hydrogen bond life times with D132

(compare model 0100 and model 1100), however, with either of the other residues protonated no such secondary effect is observed.

For E286, in contrast, there is a trend of protonated E286 exhibiting shorter hydrogen bond life times than unprotonated E286 (compare model 0000 with 0100, model 1000 with model 1100, model 0001 with model 0101, or model 0011 with model 0111 in Table S1). The longest hydrogen bond life times for E286 are observed in models 0001 and 1000 (see Table S1).

Hydrogen bond dynamics of protonated E101 is faster (shorter hydrogen bond life times) than those with unprotonated E101. An opposite effect is, however, observed for models 0110 and 0111 exhibiting hydrogen bond life times in the 0111 model that are significantly longer than in any other model.

K362's hydrogen bond dynamics show no clear dependence on this residue's protonation state, exhibiting also considerable errors in some cases and rendering this analysis difficult. The models with longest hydrogen bond life times with K362, however, can be clearly identified as model 1110 and model 1101. The fitted autocorrelations function (Fig. 3) generally show a slower decay for protonated than for unprotonated K362.

Interestingly, the hydrogen bond dynamics of the D-channel residue N139 seems to be affected by the protonation states of the other key residues, albeit more by the combination of their protonation states rather than by a single residue's protonation alone. The largest effect on the hydrogen bond life times for N139 upon changing only one residue's protonation state can be observed for E286. Models with protonated E286 exhibit shorter hydrogen bond life times for N139 than those with unprotonated E286 (compare model 0001 with model 0101, model 0011 with model 0111, or model 1010 with model 1110 in Table S1). Models with protonated K362 show significantly altered hydrogen bond dynamics of N139, compared to models with unprotonated K362. In particular, models in which D132 is also protonated exhibit longer life times for hydrogen bonds with N139 (compare model 1000 with 1010, and model 1100 with model 1110, respectively, in Table S1). If E286 is protonated instead of D132, the opposite effect is observed, i.e. hydrogen-bond life times

for N139 are reduced upon K362 protonation (compare model 0100 with model 0110 in Table S1). Comparison of models 0001 with model 0011 and model 0101 with model 0111 in Fig. 3 furthermore shows a slower decay of the hydrogen bond autocorrelation for the model with protonated K362. E101 has no clear impact on the hydrogen bond dynamics of N139.

Conformational Analysis

The conformational dynamics of important D- and K-channel residues in cytochrome c oxidase have been analyzed in terms of their side chain dihedral angles and distances between pairs of residues. Histograms of the dihedral distributions are shown in the supplementary material, see Figures S13 to S26. Fig. 4 summarizes the conformational states that are most populated in the different models.

The protonation state of D132 directly influences the side-chain conformations of this residue. Unprotonated D132 exhibits more conformations than protonated D132, in particular in side chain dihedral angle χ_1^{D132}. Models in which both, D132 and E286, are unprotonated (0000, 0001, 0010, and 0011), show an additional population with $\chi_1^{D132} \approx +60^\circ/\chi_2^{D132} \approx \pm 120^\circ$, whereas the combination of unprotonated D132 and protonated E286 results in population of states with $\chi_1^{D132} \approx 180^\circ$. The protonation states of K362 and E101, in contrast, do not influence the conformational states of D132. The $\chi_1^{D132} \approx -60^\circ/\chi_2^{D132} \approx -60^\circ$ and $\chi_1^{D132} \approx -60^\circ/\chi_2^{D132} \approx 120^\circ$ conformations are populated in all models.

E286 shows rather restricted conformational dynamics. Only three out of the nine $\chi_2^{E286}/\chi_3^{E286}$ combinations are observed. The $\chi_1^{E286} \approx 180^\circ$ is reached in all models but with protonated E286 limited to $\chi_2^{E286} \approx 60^\circ/\chi_3^{E286} \approx 0^\circ$ in which E286 is bend down into the D-channel. An exception is model 0111 that also shows states with E286 pointing upwards. Models with D132 and E286 unprotonated occupy only the $\chi_2^{E286} \approx 60^\circ/\chi_3^{E286} \approx -120^\circ$ conformation.

K362 exhibits large conformational flexibility in its sidechain, with a preference for $\chi_1^{K362} = -60^\circ/\chi_2^{K362} = 180^\circ$ in all models. Models 0111 and model 1110 are the only models in which an

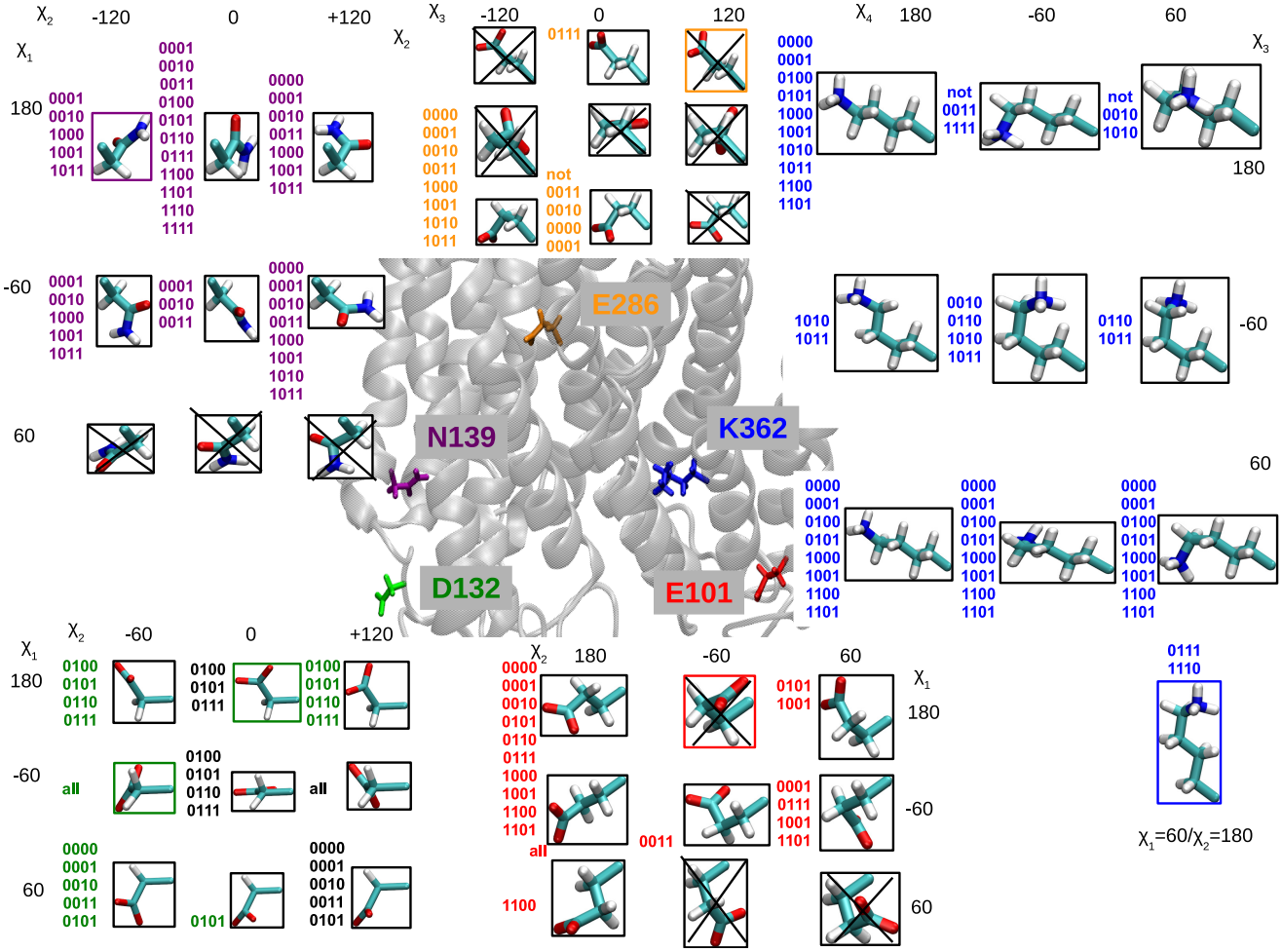

Figure 4: Dihedral conformational states of residues D132 (green), N139 (purple), E286 (orange), K362 (blue), and E101 (red). The orientation shown for each residue corresponds to the one viewed from the same perspective as the one for the protein cartoon in the center. Next to each state those protonation models for which the state has been observed in at least two of the simulation are listed. Crossed out states have not been observed in any model. For simplicity, sidechain dihedral χ_1 of E286 ($\chi_1 = 180^\circ$) and χ_3 of E101 ($\chi_3 = -120^\circ$) are shown in their most probable orientations for all models. K362 is shown with a conformation $\chi_1^{K362} = -60^\circ/\chi_2^{K362} = 180^\circ$ that is occupied in all models. Models 0111 and 1110 adopt an additional $\chi_1^{K362} \approx 60^\circ/\chi_2^{K362} \approx 180^\circ$conformation which is shown separately. The protonation models are labeled by "1" for protonated and "0" for unprotonated D132, E286, K362, and E101, respectively.

additional $\chi_1^{K362} = 60^\circ/\chi_2^{K362} = 180^\circ$ conformation is observed (see Fig. 4). There is no obvious dependence on K362's protonation state for χ_4^{K362}. $\chi_3^{K362} = 60^\circ$conformations are observed for all models with neutral K362, whereas $\chi_3^{K362} = -60^\circ$conformations are populated only in a few models with protonated K362. (cf. Fig. 4).

Sidechain conformations of E101 show little dependence on this residue's protonation state. Conformations with $\chi_1^{E101} \approx 180^\circ/\chi_2^{E101} \approx 60^\circ$ or $\chi_1^{E101} \approx -60^\circ/\chi_2^{E101} \approx 60^\circ$ are occupied in two or four models with protonated E101, respectively. However, the difference in the histograms for E101's dihedral angles between individual simulation runs, as used for error estimates, is larger in models with protonated E101 than with unprotonated E101. Neither the protonation state of K362 nor those of D-channel residues have a significant impact on the conformation of E101.

N139 is not a titratable residue itself but exhibits conformational dependence on the protonation state of the other residues. Hereby, the protonation state of E286 seems to be of utmost importance in terms of flexibility and conformations passed through. Indeed, models with unprotonated E286 occupy more different dihedral states than those with protonated E286. All models with protonated E286 occupy only the $\chi_1^{N139} \approx 180^\circ/\chi_2^{N139} \approx 0^\circ$. In contrast, states with $\chi_2^{N139} \approx 0^\circ$ are not visited by models with protonated D132 (and unprotonated E286). A conformation with $\chi_1^{N139} \approx 60^\circ$ is not observed in any of the sixteen models.

Communication between protein residues

This section reports communication pathways for which the cost of shortest paths between important residues is significantly lower than their characteristic path length. Those shortest paths can be considered to allow communication above the average or noise level.

Generalized correlation

The generalized correlation matrices presented in Fig. 5 show those of the protonation models with the most non-negligible entries and the strongest communication between key residues (see

also Table 1): model 0010, 0111, 1010, and model 1110. For the other models see supplementary Fig. S27.

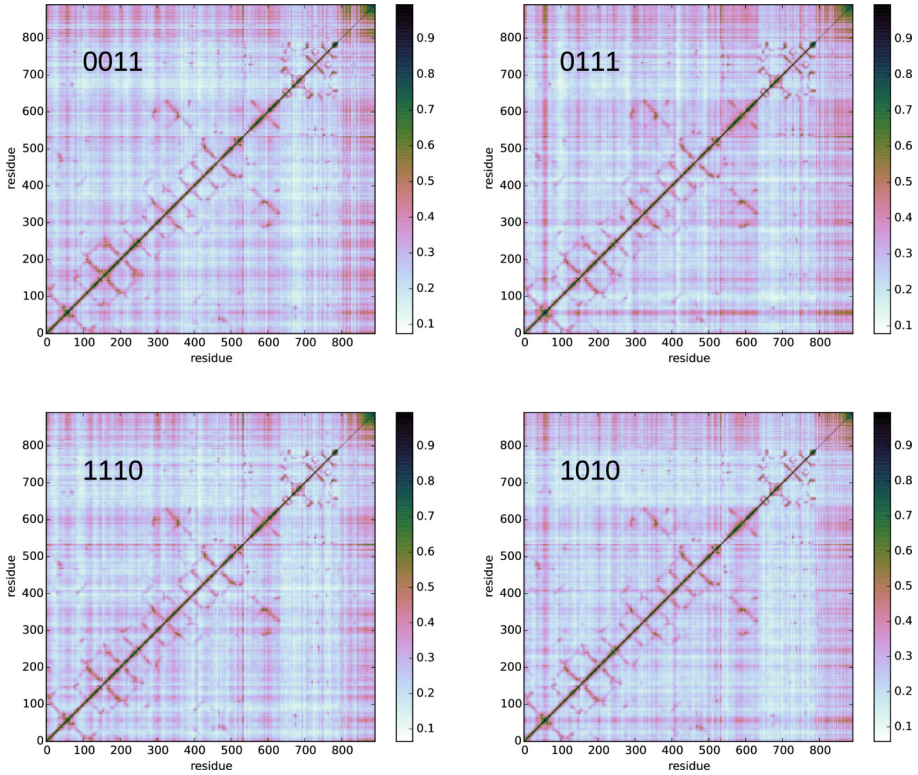

Figure 5: Generalized residue-residue correlation matrix of Cytochrome c Oxidase in the protonation state models that show largest correlations. For the other models see supplementary figure S27. The protonation models are labeled by "1" for protonated and "0" for unprotonated D132, E286, K362, and E101. The values of the matrix elements, i.e. the generalized correlations coefficients $r_{MI}[x_i, x_j]$, are color coded as indicated by the color bars plotted next to the matrices.

These four models also show strongest communication for almost all pathways analysed (see Table 1). Models 0111 and 0010 are, moreover, the models with the shortest characteristic path length (see Table S2), indicating an average connection that is stronger than in the other models.

Within the D-channel, strongest communication is observed for models with protonated E286. Whereas D132 and N139 communicate strongly in all models analysed, likely because they are close to each other, communication between N139 and the more distant E286 is only moderate in almost all models. The shortest communication paths between N139 and E286 are observed for models 0010, 0111 and 1110, the latter two of which have E286 protonated. The farther communication

Table 1: Communication paths between selected residues in Cytochrome c Oxidase. Only the models with lowest path costs are listed. The cost or length of a shortest path $P(v_1, \ldots, v_n)$ is the sum of the edge weights along that path, here $\sum_{k=1}^{n} -\ln(R_{k,k+1})$ where $R_{k,i+1}$ is the generalized correlation as defined in eq. 1. For N139 to E101 no shortest path with a cost below the characteristic path length could be obtained. The protonation models are labeled by "1" for protonated and "0" for unprotonated D132, E286, K362, and E101, respectively.

Path	Model (shortest path length (cost))							
E286-D132	1110	(2.1±0.36)						
N139-D132	1110	(0.7±0.07)						
E286-N139	0010	(1.7±0.15)	0111	(1.7±0.2)	1110	(1.7±0.2)		
Y288-E101	0111	(1.6±0.7)						
K362-Y288	1110	(1.1±0.08)	0111	(1.1±0.3)				
K362-E101	0111	(0.8±0.3)						
K362-D132	1110	(2.4±0.18)	0110	(2.4±0.25)	1010	(2.4±0.4)		
K362-N139	1110	(2.5±0.26)						
K362-E286	1110	(1.5±0.09)	0111	(1.5±0.5)	0010	(1.6±0.17)	1011	(1.6±0.4)
Y288-D132	1110	(2.2±0.33)						
D132-E101	0111	(2.5±0.4)						
N139-E101				-				
E286-E101	0111	(2.0±0.8)	1110	(2.1±0.30)				

between E286 and the other terminal residue of the D-channel, D132, is noteworthy only for model 1110.

Communication between the central K-channel residue K362 and the terminal residues of this channel, E101 and Y288, respectively, is rather strong in almost all models which can be attributed to their relatively short distance. In contrast, the two termini Y288 and E101 show significant communication only in model 0111.

Inter-channel communication is mainly from K362 to the D-channel residues. K362 and E286 exhibit strongest communication in those models that also show the shortest communication paths between the D-channel termini, these are 1110, 0111, 1010, and 1011. There is only weak communication between K362 and N139 in model 1110. Models 1110, 0110, and 1010 also communicate weakly, between K362 and D132. No significant communication is observed between the entrance residues of the two channels, D132 and E101, only weak in model 0111. In the most "talkative" models, however, 0111 and 1110, there is communication between the D-channel residue E286 and

K-channel residue E101 which is remarkably because of the rather large distance between the two residues. Y288-D132 communication is moderate only in model 1110

It is interesting to note that K362 is protonated in all the models that exhibit strong communication via generalized correlation.

Hydrogen Bond Interactions

Table 2: Hydrogen-bond paths with strong communication between selected residues in Cytochrome c Oxidase. Only the models with lowest path costs are listed. The cost or length of a shortest path $P(v_1, \ldots, v_n)$ is the sum of the edge weights along that path, here $\sum_{k=1}^{n} -\ln(H_{k,k+1})$ where $H_{k,k+1}$ is the strength of a hydrogen-bond connection between k and $k+1$. The strength of the hydrogen-bond connection is given by its length and its probability to be formed (see Methods section). For D132 to K362, D132 to E101, and N139 to E101 no shortest paths with a cost below the characteristic path length could be obtained. The protonation models are labeled by "1" for protonated and "0" for unprotonated D132, E286, K362, and E101, respectively.

Path	Models (shortest path length (cost))					
E286-D132	1100	(16.9±2.7)	1111	(17.1±1.8)		
N139-D132	1100	(7.7±1.7)	0101	(8.1±1.3)		
E286-N139	1111	(10.8±1.9)	1100	(11.0±1.8)	0100(11.1±0.7)	0110(11.2±1.3)
Y288-E101	0000	(12.1±2.8)	0100	(12.8±3.5)		
K362-Y288	1000	(3.5±0.2)				
K362-E101	0000	(7.1±1.1)	0100	(7.7±1.3)		
K362-D132				-		
K362-N139	0100	(14.8±2.0)	1001	(15.0±1.7)	1101(15.3±3.0)	
K362-E286	0100	(7.4±1.9)	1000	(7.6±0.3)		
Y288-D132	1100	(17.4±4.0)				
D132-E101				-		
N139-E101				-		
E286-E101	0100	(15.2±2.9)	0000	(16.7±3.4)		

Table 2 lists the models with shortest paths for communication via hydrogen-bonds. Intra-channel communication between the terminal residues of the D-channel, i.e. between D132 and E286 is observed only in two cases: for model 1100 and 1111, both of which have both terminal residues protonated, but rather weak. Communication between N139 and D132 is strong in two models, 1100 and 0101, without obvious dependence on the residues' protonation state. The

hydrogen bond communication between N139 and E286, in contrast, is strongest for models with protonated E286.

In the K-channel, communication of K362 and Y288, which can be considered the upper half of the channel, is very strong in all models investigated. Similarly, communication between E101 and K362 is also strong, and strongest in models with both these residues K362 and E101 unprotonated. Interestingly, communication between the terminal residues of the K-channel, i.e. E101 and Y288, is only moderate, but strongest in the same models that exhibit strong communication between K362 and E101, 0000 and 0100, in which the shortest communication paths run via K362. And communication between K362 and E286 is strong for all models considered that have K362 unprotonated. The strongest such communication is found in models 0100 and 1000. Also inter-channel communication between K362 and N139 shows shortest paths via hydrogen-bond connectionsfor unprotonated K362 but at moderately elevated cost. No strong inter-channel communication can be observed between E101 and the D-channel residues D132 or N139. Between E101 and E286 there is weak communication for models 0100 and 0000 that again follows paths via K362. Only weak communication can be observed between Y288 and D132 for model 1100.

In general, the models which show strongest communication via hydrogen bonds are different from those that communicate strongly via correlated motions.

Discussion

The hydrogen-bond dynamics of the key residues analyzed in this work show a dependence on the residues' own protonation state (except for D132) and in some cases they are also affected by the protonation states of the other residues.

Within the K-channel a slower decay of the hydrogen bond autocorrelation function is observed for protonated K362. No mutual impact on their hydrogen-bond dynamics can be observed between K362 and the terminal K-channel residue, E101. There is however, communication between the

two residues along correlations if both are protonated and via hydrogen-bond connections if both residues are unprotonated. This may be traced back to protonated K362 pointing preferably "up", that is away from E101, and hence having less impact on the hydrogen bonded network of E101.

Within the D-channel, the mutual impact of key residues is also protonation state dependent. The conformational preference of E286 for "down", i.e. towards the D-channel or "up" has been reported to depend on its protonation state as well as on the redox state of the protein and the hydration level of water cavities[34]. Whereas the P_M state of CcO in which heme a is reduced and the BNC site is oxidized shows no preference for "up" or "down" in protonated E286, the "down" conformation is preferred after moving an electron from heme a to the BNC (P_R state)[34]. According to the MD simulations of the $P_R \rightarrow$F intermediate performed in this work, the "down" conformation of E286 is also preferred, independent of the protonation state of E286. The "up" conformation, however is only observed for one model with protonated E286, model 0111. Molecular dynamics simulations of Cytochrome c Oxidase from bovine heart also find a preference for a "down" conformation at least with protonated E286 and little to no water in the cavity above E286.

The conformational dynamics of both D-channel residues, D132 and E286, mainly depend on their own protonation state. However, protonated E286 leads to D132 exploring more dihedral conformations corresponding to an "upwards" orientation towards the D-channel interior. And protonated D132, in turn, results in the occupation of an additional dihedral state by E286.This slight preference for conformations toward each other is in agreement with the weak communication between D132 and E286 (hydrogen-bond or correlation based), that is only observed in models which have both D-channel residues protonated. The hydrogen-bond dynamics of the two residues, D132 and E286, are not affected by the protonation state of the other residue, being rather diverse for D132 anyway.

The conformational dynamics of the non-titratable residue N139 is clearly affected by protonation of E286. Furthermore, hydrogen-bonded communication between these two residues is

considerable in models with at least one of D132 or E286 protonated and strongest in those models which have both terminal residues of the D-channel protonated. These are the same models that also show weak hydrogen bond communication along the entire D-channel, i.e. between E286 and D132. Single protonation of D132, on the other hand, does not exhibit any particular effect on N139.

According to free energy calculations by Henry et al[35], N139 can be found in two distinct states where the global minimum conformation is a "closed" state ($\chi_1^{N139} = -165^\circ/\chi_2^{N139} = 41^\circ$) that would not allow water molecules and likely neither protons to pass. Another slightly less favorable metastable conformation, called the "open" state (with $\chi_1^{N139} = -75^\circ/\chi_2^{N139} - 70^\circ$) would, in contrast, favor water and proton transfer. The conformational analysis performed here, confirms these states. The $\chi_1^{N139} \approx 180^\circ/\chi_2^{N139} \approx 0^\circ$conformations observed in our simulations correspond to the "closed" state and the $\chi_1^{N139} \approx -60^\circ/\chi_2^{N139} \approx +120^\circ$conformations to an "open" state, respectively. The "open" state observed here, however, is different from the one observed by Henry et al[35] by a swap of the OD and NH2 atoms of the asparagine side chain (cf. $\chi_2^{N139} \approx +120^\circ$ and $\chi_2^{N139} \approx -70^\circ$) but more similar to the rotamer assigned in the crystal structure. Our analysis furthermore indicates a conformational dependence on the protonation state of E286. All models with protonated E286 significantly favor a state with N139 "closed" with only models 1100 and 1110 showing a low population of the "open" state in more than one of the MD runs. In contrast, models with unprotonated E286 exhibit more conformational flexibility in N139 such that the "open" state is also significantly populated. This "open" state is a prerequisite for the formation of a hydrogen-bonded water chain that enables proton transfer in a Grotthuss mechanism[36]. Furthermore, models with protonated E286 exhibit shorter life times for hydrogen bonds between N139 and water molecules. N139 can therefore indeed be regarded to have a gating role in the D-channel, allowing proton passage only for unprotonated E286 and thus preventing an additional, excess proton close to E286 and premature release of a proton out of the D-channel.

The hydrogen-bond dynamics of N139 also depend on the protonation state of K362, but the

direction of the effect (slower or faster) also depends on the protonation states of the other D-channel residues. In models with protonated D132, K362 protonation results in longer hydrogen bond life times for N139, but when E286 is protonated (and D132 is not) these life times are shorter for models with protonated K362.

For models with unprotonated E286, in which N139 significantly samples "open" conformations, increased hydrogen bond life times for N139 in models with protonated K362 can be interpreted as an increased probability for proton transfer from the protonated D132 along hydrogen bonds with an increased and thus sufficiently long life time. In situations with protonated E286, on the other hand, the shorter hydrogen bond life times for N139 and its preference for "closed" conformations prevents proton transport through the D-channel. Consequently, proton release from E286 to the proton loading site or to the BNC likely takes place before proton uptake through the D-channel.

Further implications on the proton transfer process, however, cannot be deduced from the present simulations. Molecular dynamics simulations of Cytochrome c Oxidase and other proteins with water channels have revealed a significant change of the water network and water-wire structures upon changes in the electrostatic environment by protonation or changes in the redox state that are not captured in the present classical simulations[37–39]. In particular the location of an excess proton on a water molecule has not been considered in this work. The altered water-wire structure, caused by protonated water (as opposed to the protonated protein residues investigated here) will is likely also have considerable impact on the hydrogen and dynamics and the communication within and between the two channels of Cytochrome c Oxidase.

Moreover, it has been observed that the presence of an excess proton in channel-like environments (such as carbon nanotubes) has a "wetting" effect, i.e. results in an increased number of water molecules inside the channel and therefore in a significant change of the water network[40]. In previous MD simulations[11] and in those presented in this work such an is indeed effect is observed. Models with protonated K362 exhibit a larger number of water molecules inside the K-channels, i.e. close to K362, than those with unprotonated K362 (see Figure S28). However, models with a

simultaneously protonated E101 generally show a diminished effect.

Interestingly, the communication between K362 and N139 is rather weak. Via correlated motions it is noteworthy only in a model with protonated K362 (1110). And the communication via hydrogen-bond connections is somewhat stronger in models with unprotonated K362 than in those with protonated K362. The rather long-range effect of K362 on the hydrogen-bond dynamics of N139 must therefore follow other pathways. The communication between E286 and K362, in contrast, is rather strong via hydrogen-bonds and also notable via correlations. It is therefore conceivable that the effect of a protonated K362 on N139 hydrogen-bond dynamicsassisted by E286. The distance of K362 to both residues, N139 and E286, exhibits longer and shorter values, respectively, with protonated K362. While also the shorter distances are still rather long for direct electrostatic interactions, they likely impact also the conformations and interactions of other residues, i.e. water, in between.

The means of communication between the different key residues analyzed, also appears to be protonation state dependent. All strongest communication pathways via correlated motions are observed for models with protonated K362. The models which show significant generalized correlation (see Fig. 5) are 0111, 1110, 0010, and 1010. Consequently, these are the models which have the shortest paths between residues at lowest cost. All these models also have an increased number of water molecules inside the K-channels along which communication can take place. Along generalized correlation, for those models, communication is observed between residues of the same channel as well as inter-channel communication. Models with protonated K362 exhibit additional "up" conformations that are no observed in models with unprotonated K362, thereby likely impacting more different residues, and facilitating communication between them. In the two models with strongest communication via correlations, 0111 and 1110, yet another conformation of K362's sidechain dihedral angle $\chi_1 \approx 60°$ can be observed in at least one of the individual MD runs, supporting the idea that conformational flexibility enhances communication. The "most talkative" models via hydrogen-bonds, 0100 and model 1100, have K362 unprotonated. These

models communicate only via hydrogen bond connections.

The communication between both proton conducting channels in Cytochrome c Oxidase is most pronounced in the 0111 or 1110 system. In both these systems a proton would be ready to leave either channel towards the PLS or the BNC, respectively. However, to function properly, i.e. act as oxidase and as a proton pump, the proton needs to be transferred from the D-channel, of CcO[41] likely towards the PLS[42] to be later on expelled to the P-side. Protonated K362 influences the hydrogen bond dynamics of N139 within the D-channel of CcO such that it elongates the hydrogen bond lifetimes compared to states with unprotonated K362, possibly facilitating the proton transfer through the D-channel, as long as E286 is not yet protonated. This effect is further supported by the conformational preference for "open" states of N139 with unprotonated E286. One can therefore assume that a protonated K362 supports the proton transfer through the D-channel.

Conclusions

Conformational dynamics, hydrogen bond dynamics as well as communication of residues in both channels of Cytochrome c Oxidase depend on the combination of their protonation states rather than on the protonation state of a single residue. In particular, communication within the same channel is dependent on the protonation states of all the key residues of that channel. In addition to the titratable residues themselves, also the conformational dynamics of the D-channel residue N139 are affected by the protonation state of the other D-channel residues, resulting in a gating role of N139. A mutual impact of the two channels is mainly observed on the hydrogen bond dynamics, in particular on K362 and N139. Intra-channel communication is mainly via correlated motions, suggesting an interplay of protein residue and water motion with hydrogen bond life times. The protonation state of K362 likely affects the proton transfer probabilities in the D-channel via the hydrogen bond dynamics of N139, acting in concert with the protonation states of the D-channel termini. Formation of long-lived hydrogen-bonded water wires allowing proton relay to E286 are

only observed when this residue is unprotonated and proton transport to it still has to take place.

In addition to the strength, also the means of communication is protonation state dependent. For example, communication changes from mainly hydrogen-bonded connections in unprotonated K362 to correlation-based communication for protonated K362.

The states that have E286 protonated can be understood as states ready to release protons. Reaching such a state is more likely with protonated than with unprotonated K362. The protonation-state dependent communication between the two channels may thus also regulate proton release from the D-channel and the completion of the $P_R \rightarrow F$ transition.

Author Contributions

P.I. and A.L.W. designed research; M.H.B., T.G., and P.I. performed research; M.H.B., T.G., and R.M. analyzed data, M.H.B., T.G., E.W.K, and P.I. wrote the manuscript.

Acknowledgement

We thank the Deutsche Forschungsgemeinschaft (DFG) for financial support provided to the Sonderforschungsbereich 1078 (SFB 1078) on 'Protonation Dynamics in Protein Function'. We are grateful for computational resources provided by the North-German Supercomputing Alliance (HLRN) and the Zedat cluster "Soroban" of the Freie Universität Berlin. IT support by Jens Dreger of the Physics department at Freie Universität Berlin is gratefully acknowledged.

References

(1) Babcock, G. T.; Wikström, M. Oxygen activation and the conservation of energy in cell respiration. *Nature* **1992**, *356*, 301–309.

(2) Ädelroth, P.; Gennis, R. B.; Brzezinski, P. Role of the pathway through K (I-362) in proton transfer in cytochrome c oxidase from R. sphaeroides. *Biochemistry* **1998**, *37*, 2470–2476.

(3) Konstantinov, A. A.; Siletsky, S.; Mitchell, D.; Kaulen, A.; Gennis, R. B. The roles of the two proton input channels in cytochrome c oxidase from Rhodobacter sphaeroides probed by the effects of site-directed mutations on time-resolved electrogenic intraprotein proton transfer. *Proc. Nat. Acad. Sci. U.S.A.* **1997**, *94*, 9085–9090.

(4) Brzezinski, P.; Adelroth, P. Proton-controlled electron transfer in cytochrome c oxidase: functional role of the pathways through Glu 286 and Lys 362. *Acta Physiol. Scand. Supplementum* **1998**, *643*, 7–16.

(5) Vygodina, T.; Pecoraro, C.; Mitchell, D.; Gennis, R.; Konstantinov, A. Mechanism of inhibition of electron transfer by amino acid replacement K362M in a proton channel of Rhodobacter sphaeroides cytochrome c oxidase. *Biochemistry* **1998**, *37*, 3053–3061.

(6) Sharpe, M. A.; Ferguson-Miller, S. A chemically explicit model for the mechanism of proton pumping in heme–copper oxidases. *J. Bioener. Biomembran.* **2008**, *40*, 541–549.

(7) Iwata, S.; Ostermeier, C.; Ludwig, B.; Michel, H. Structure at 2.8 Å resolution of cytochrome c oxidase from Paracoccus denitrificans. *Nature* **1995**, *376*, 660–668.

(8) Namslauer, A.; Lepp, H.; Brändén, M.; Jasaitis, A.; Verkhovsky, M. I.; Brzezinski, P. Plasticity of proton pathway structure and water coordination in cytochrome c oxidase. *J. Biol. Chem.* **2007**, *282*, 15148–15158.

(9) Ostermeier, C.; Harrenga, A.; Ermler, U.; Michel, H. Structure at 2.7 Å resolution of the Paracoccus denitrificans two-subunit cytochrome c oxidase complexed with an antibody FV fragment. *Proc. Nat. Acad. Sci.* **1997**, *94*, 10547–10553.

(10) Hofacker, I.; Schulten, K. Oxygen and proton pathways in cytochrome c oxidase. *Proteins* **1998**, *30*, 100–107.

(11) Woelke, A. L.; Galstyan, G.; Knapp, E.-W. Lysine 362 in cytochrome c oxidase regulates opening of the K-channel via changes in pKA and conformation. *Biochim. Biophys. Acta (BBA) - Bioenergetics* **2014**, *1837*, 1998 – 2003.

(12) Brändén, M.; Sigurdson, H.; Namslauer, A.; Gennis, R. B.; Ädelroth, P.; Brzezinski, P. On the role of the K-proton transfer pathway in cytochrome c oxidase. *Proc. Nat. Acad. Sci. U.S.A.* **2001**, *98*, 5013–5018.

(13) The role of the K-channel and the active-site tyrosine in the catalytic mechanism of cytochrome c oxidase. *Biochimica et Biophysica Acta (BBA) - Bioenergetics* **2016**, *1857*, 1111 – 1115.

(14) Morgan, J. E.; Verkhovsky, M. I.; Palmer, G.; Wikström, M. Role of the PR Intermediate in the Reaction of Cytochrome c Oxidase with O2. *Biochemistry* **2001**, *40*, 6882–6892.

(15) Brändén, M.; Tomson, F.; Gennis, R. B.; Brzezinski, P. The entry point of the K-proton-transfer pathway in cytochrome c oxidase. *Biochemistry* **2002**, *41*, 10794–10798.

(16) Tomson, F. L.; Morgan, J. E.; Gu, G.; Barquera, B.; Vygodina, T. V.; Gennis, R. B. Substitutions for Glutamate 101 in Subunit II of Cytochrome c Oxidase from Rhodobacter sphaeroides Result in Blocking the Proton-Conducting K-Channel. *Biochemistry* **2003**, *42*, 1711–1717.

(17) MacKerell, Jr., A. D. et al. All-Atom Empirical Potential for Molecular Modeling and Dynamics Studies of Proteins. *J. Phys. Chem. B.* **1998**, *102*, 3586 –3616.

(18) Jorgensen, W. L.; Chandrasekhar, J.; Madura, J. D.; Impey, R. W.; Klein, M. L. Comparison of simple potential functions for simulating liquid water. *J. Chem. Phys.* **1983**, *79*, 926–935.

(19) Klauda, J. B.; Venable, R. M.; Freites, J. A.; O'Connor, J. W.; Tobias, D. J.; Mondragon-Ramirez, C.; Vorobyov, I.; Jr., A. D. M.; Pastor, R. W. Update of the CHARMM all-atom additive force field for lipids: validation on six lipid types. *J. Phys. Chem. B* **2010**, *114*, 7830–7843.

(20) Darden, T.; York, D.; Pedersen, L. G. Particle mesh Ewald: an Nlog(N) method for Ewald sums in large systems. *J. Chem. Phys.* **1993**, *98*, 10089–10092.

(21) Ryckaert, J.-P.; Ciccotti, G.; Berendsen, H. J. C. Numerical integration of the cartesian equations of motion of a system with constraints: molecular dynamics of n-alkanes. *J. Comp. Phys.* **1977**, *23*, 327–341.

(22) Phillips, J. C.; Braun, R.; Wang, W.; Gumbart, J.; Tajkhorshid, E.; Villa, E.; Chipot, C.; Skeel, R. D.; Kale, L.; Schulten, K. Scalable molecular dynamics with NAMD. *J. Comput. Chem.* **2005**, *26*, 1781–1802.

(23) Lange, O. F.; Grubmüller, H. Generalized Correlation for Biomolecular Dynamics. *PROTEINS: Structure, Function, and Bioinformatics* **2006**, *62*, 1053–1061.

(24) Cover, T. M.; Thomas, J. A. *Elements of Information Theory*; John Wiley & Sons: New York, 2006; p 19.

(25) Kraskov, A.; Stögbauer, H.; Grassberger, P. Estimating mutual information. *Phys. Rev. E* **2004**, *69*, 066138.

(26) Dijkstra, E. A note on two problems in connexion with graphs. *Num. Math.* **1959**, *1*, 269–271.

(27) Bagga, J.; Heinz, A. In *Graph Drawing*; Mutzel, P., Jünger, M., Leipert, S., Eds.; Lecture Notes in Computer Science; Springer Berlin Heidelberg, 2002; Vol. 2265; pp 459–460.

(28) Stillinger, F. H. Water Revisited. *Science* **1980**, *209*, 451–457.

(29) Luzar, A.; Chandler, D. Hydrogen-Bond Kinetics in Liquid Water. *Nature* **1996**, *379*, 55–57.

(30) Baker, E. N.; Hubbard, R. E. Hydrogen Bonding in Globular Proteins. *Prog. Biophys. Mol. Biol.* **1984**, *44*, 97–179.

(31) Levitt, M.; Sharon, R. Accurate Simulation of Protein Dynamics in Solution. *Proc. Natl. Acad. Sci. U. S. A.* **1988**, *85*, 7557–7561.

(32) Rapaport, D. C. Density Fluctuations and Hydrogen Bonding in Supercooled Water. *Mol. Phys.* **1983**, *48*, 23–31.

(33) Luzar, A. Resolving the Hydrogen Bond Dynamics Conundrum. *J. Chem. Phys.* **2000**, *113*, 10663–10675.

(34) Kaila, V. R.; Verkhovsky, M. I.; Hummer, G.; Wikström, M. Glutamic acid 242 is a valve in the proton pump of cytochrome c oxidase. *Proc. Nat. Acad. Sci. U.S.A.* **2008**, *105*, 6255–6259.

(35) Henry, R. M.; Yu, C.-H.; Rodinger, T.; Pomès, R. Functional Hydration and Conformational Gating of Proton Uptake in Cytochrome c Oxidase. *J. Mol, Biol.* **2009**, *387*, 1165 – 1185.

(36) Grotthuss, C. D. Memoir on the decomposition of water and of the bodies that it holds in solution by means of galvanic electricity. *Biochim. Biophys. Acta (BBA)-Bioenergetics* **2006**, *1757*, 871–875.

(37) Xu, J.; Sharpe, M. A.; Qin, L.; Ferguson-Miller, S.; Voth, G. A. Storage of an excess proton in the hydrogen-bonded network of the D-pathway of cytochrome c oxidase: identification of a protonated water cluster. *J. Am. Chem. Soc.* **2007**, *129*, 2910–2913.

(38) Lee, H. J.; Svahn, E.; Swanson, J. M.; Lepp, H.; Voth, G. A.; Brzezinski, P.; Gennis, R. B. Intricate Role of Water in proton transport through cytochrome c oxidase. *J. Am. Chem. Soc.* **2010**, *132*, 16225–16239.

(39) Yamashita, A.; Voth, G. A. Insight into the mechanism of Proton transport in Cytochrome c Oxidase. *Journal of the American Chemical Society* **2011**, *134*, 1147–1152.

(40) Peng, Y.; Swanson, J. M.; gu Kang, S.; Zhou, R.; Voth, G. A. Hydrated excess protons can create thei own water wires. *J. Phys. Chem. B* **2014**, *119*, 9212–9218.

(41) Wikström, M.; Sharma, V.; Kaila, V. R. I.; Hosler, J. P.; Hummer, G. New Perspectives on Proton Pumping in Cellular Respiration. *Chem. Rev.* **2015**, *115*, 2196–2221.

(42) Belevich, I.; Bloch, D. A.; Belevich, N.; Wikström, M.; Verkhovsky, M. I. Exploring the proton pump mechanism of cytochrome c oxidase in real time. *Proc. Nat. Acad. U.S.A.* **2007**, *104*, 2685–2690.